Experimental ^{1}H NMR and Computational Studies of Internal Rotation of Solvated Formamide

Angela N. Taha and Nancy S. True*

Chemistry Department, University of California, Davis, California 95616

Received: November 5, 1999; In Final Form: January 27, 2000

Solvent effects on the C−N bond rotation process of formamide (FA) are investigated experimentally and theoretically. Temperature-dependent exchange broadened ^{1}H NMR line shapes of [^{15}N]FA in water, dimethyl sulfoxide-d_6, and tetrachloroethane-d_2, and as neat solution are consistent with $\Delta G^{\ddagger}_{298}$ values for FA internal rotation, in kilocalories per mole, of 18.2(0.1), 17.8(0.1), 17.2(0.1), and 18.0(0.1), respectively. These values are significantly higher than the gas-phase $\Delta G^{\ddagger}_{298}$ value, 16.0(0.1) kcal mol^{-1}, and they correlate well with empirical spectroscopic solvent polarity scales. Self-consistent isodensity polarizable continuum model (SC-IPCM) calculations at the HF/6-311++G** level of theory for FA in a series of dielectric constants ranging from 1 to 109 predict a complete reversal of the preferred internal rotation path for hydrated FA compared to gas-phase FA. Equal contributions to the internal rotation rate constant from both possible internal rotation paths is predicted to occur at a dielectric constant of 7.08. SC-IPCM calculations predict that $\Delta G^{\ddagger}_{298}$ for hydrated FA is 1.99 kcal mol^{-1} higher than $\Delta G^{\ddagger}_{298}$ for gas-phase FA. SC-IPCM calculations for a 1:1 FA−H_2O complex were performed to allow for direct inclusion of intermolecular hydrogen bonding. The predicted $\Delta G^{\ddagger}_{298}$ for the hydrated 1:1 FA−H_2O complex is ca. 2.3 kcal mol^{-1} higher than the predicted gas-phase $\Delta G^{\ddagger}_{298}$, in excellent agreement with experiment.

Introduction

Formamide (FA) continues to receive considerable experimental and theoretical attention due to its fundamental importance as the building block of proteins and enzymes[1,2] and because it is the simplest model to use to investigate hydration in molecules containing the amide functional group.[3] In addition to its biological importance, the internal rotation process of FA is intrinsically interesting. It can undergo internal rotation via two distinct transition states which are close in energy but significantly different in polarity, and five of the six atoms in this molecule can participate in hydrogen bonding. Also slow intramolecular vibrational redistribution (IVR) may be an important consideration in the kinetic description of the internal rotation process since FA is a small molecule and it undergoes internal rotation at internal energies where its vibrational state density is low.

Internal rotation of FA is a frequent topic of computational studies, many of which are aimed at developing methods to predict solvent effects on intramolecular processes.[4−10] Presently available experimental data[11−13] show qualitative trends in solvent effects on the internal rotation barrier of FA but do not provide a good quantitative test of the theoretical predictions that have been reported. We recently measured the internal rotation barrier of FA in the gas phase[14] as a first step in determining the magnitude of the solvent effects on the system. However, most solution phase data were obtained over 25 years ago using samples containing high FA concentrations and data reduction methods which can result in significant systematic errors. The only reported $E_{act.}$ value for FA in H_2O determined from NMR measurements was reported in 1968.[12] The present study reports experimental internal rotation barriers for formamide in water and two other solvents and compares the observed solvent effects with theoretical models.

Previously reported rotational barriers of solvated FA, listed in Table 1, increase with increasing polarity and hydrogen bonding capability of the solvent.[11−13] The dependence of the FA internal rotation barrier on solvent polarity is not surprising since changes in dipole moment accompany FA internal rotation. The experimental dipole moment of the ground state is 3.714 D.[15,16] Calculations at the HF/6-311++G** level of theory predict a dipole moment of 4.218 D for the ground state and 1.662 and 4.144 D for TS1 (nitrogen lone pair anti to the carbonyl oxygen) and TS2 (nitrogen lone pair syn to the carbonyl oxygen), respectively.[17] The calculated gas-phase barriers for internal rotation proceeding via TS1 and TS2 at this level of theory are 15.26 and 18.70 kcal mol^{-1}, respectively.[17] Other calculations predict barriers ranging from 14.2 to 18.7 kcal mol^{-1} with the more recent values centered in the 15−16 kcal mol^{-1} range.[4−8,18−25] The most recent and highest level calculation (CCSD(T)/ PVTZ basis set) reported a $\Delta G^{\ddagger}_{298}$ for internal rotation via TS1 of 15.2 ± 0.5 kcal mol^{-1}, where the uncertainty is the result of the basis set dependence of the calculated vibrational frequencies.[18] No data were reported for TS2 in that study. Recent self-consistent isodensity polarizable continuum model (SC-IPCM) calculations (HF/6-31G**) reported by Craw et al. for hydrated FA predict an increase above the predicted gas-phase rotational barrier of 3.5 kcal mol^{-1} for the reaction proceeding via TS1 and a decrease of 0.1 kcal mol^{-1} for the TS2 reaction pathway.[5] They report significant changes in the geometries and potential derived charges for the ground state, TS1, and TS2 with solvation. The primary effect is an increase in electron density at the oxygen and a decrease in electron density at the carbon.

Reaction field theory does not provide a mechanism for including specific interactions such as hydrogen bonding in the calculation of the solvation energy, and an alternative approach is necessary to fully model solvent effects in systems with strong

10.1021/jp993915c CCC: $19.00
Published on Web 03/11/2000

TABLE 1: Experimental and Calculated (HF/6-311++G) Eyring Parameters for Internal Rotation of FA [$\Delta G^{\ddagger}_{298}$ and $\Delta H^{\ddagger}_{298}$ Values in kilocalories per mole and $\Delta S^{\ddagger}_{298}$ in calories per mole per kelvin][a]**

	experimental			calculated (SC-IPCM)			calculated (IPCM)		
solvent (ϵ)	$\Delta G^{\ddagger}_{298}$	$\Delta H^{\ddagger}_{298}$	$\Delta S^{\ddagger}_{298}$	$\Delta G^{\ddagger}_{298}$(TS1)	$\Delta G^{\ddagger}_{298}$(TS2)	$\Delta G^{\ddagger}_{298}$(combined)	$\Delta G^{\ddagger}_{298}$(TS1)	$\Delta G^{\ddagger}_{298}$(TS2)	$\Delta G^{\ddagger}_{298}$(combined)
gas (1)[b]	16.0(0.1)	15.8(0.6)	−0.7(0.9)	15.26	18.70	15.25	15.28	18.69	15.28
dioxane (2.21)[c]	18.0(1.4)	16.2(1.0)	−6.0(3.2)	16.58	18.11	16.54	17.08	18.56	17.03
diglyme (7.23)[d]	17.8(0.7)	19.0(0.4)	4.0(2.0)	17.65	17.63	17.23	18.09	18.65	17.89
TClE (8.50)[e]	17.2(0.1)	16.5(0.4)	−2.2(0.3)	17.73	17.59	17.25	18.17	18.66	17.95
MPK (15.45)[d]	17.8(0.7)	18.5(0.4)	2.7(2.0)	17.94	17.49	17.27	18.37	18.67	18.09
acetone (20.60)[c]	17.8(0.1)	16.3(1.9)	−5.2(5.9)	18.01	17.47	17.26	18.44	18.68	18.14
DMSO (47.27)[e]	17.8(0.1)	16.8(0.4)	−3.4(0.3)	18.13	17.41	17.26	18.55	18.69	18.21
H_2O (78.5)[c]	18.4(2.2)	20.7(1.3)	7.7(5.9)	18.17	17.39	17.24	18.59	18.69	18.23
H_2O (78.5)[e]	18.2(0.1)	18.9(0.6)	2.6(0.6)	18.17	17.39	17.24	18.59	18.69	18.23
neat (109)[c]	18.8(1.3)	18.3(1.0)	−1.7(2.7)	18.18	17.38	17.23	18.60	18.70	18.24
neat (109)[e]	18.0(0.1)	18.1(0.3)	0.2(0.2)	18.18	17.38	17.23	18.60	18.70	18.24

[a] Dielectric constants are reported at 298.15 K. [b] Reference 14. [c] Reference 12. [d] Reference 13. [e] Reference 17.

solute−solvent interactions such as aqueous amide solutions. Calculations reported by Wiberg et al. using reaction field theory and the IPCM at HF and MP2 levels of theory (using HF and MP2 optimized gas-phase geometries) of the internal rotation barriers in *N*,*N*-dimethylformamide (DMF) and *N*,*N*-dimethylacetamide[9] show qualitative agreement between the IPCM predicted barriers to rotation and the experimental values in some solvents. The agreement for hydrogen bonding solvents and solvents containing second and third row elements is poor, however. After recent application of self-consistent reaction field (SCRF) theory using IPCM to investigate solvation effects on the C−N bond rotation in (*N*,*N*-dimethylamino)acrylonitrile (DMAAN), similar deviation of the predicted and experimental barriers in these solvents was reported.[26,27]

Previous attempts to more accurately incorporate hydrogen bonding effects on FA internal rotation include QM-MM methods which model the solute quantum mechanically and the solvent with molecular mechanics. An ab initio calculation with a CCDZP basis set found that the rotation barrier of FA is increased by 1−3 kcal mol^{-1} when a single water molecule is attached.[8] Ab initio QM-MM calculations of the FA internal rotation barrier in water predict a barrier increase of 4.9 (TS1) and 2.0 kcal mol^{-1} (TS2) in comparison to calculated values for isolated FA.[5] The effective fragment potential (EFP) method has also recently been applied to hydrated FA.[7] These studies report rotational barriers for FA−H_2O complexes containing 0−5 waters. The EFP calculations predict a minimum structure for the complex that saturates at 4−5 water molecules and estimates a rotational barrier through TS1 of ca. 20 kcal mol^{-1} with electron correlation. These results agree with predicted values computed by full ab initio methods performed on complexes with 1−2 water molecules. Surprisingly, that study did not report any calculations for TS2.

An alternate approach used in the present paper to model FA in aqueous solution retains the reaction field method for incorporating the solvent dielectric contribution to the barrier and accounts for the dominant specific solute−solvent interaction by assuming that the predominant form of the reactant is the 1:1 FA−H_2O complex. This approach has been used by Wiberg et al. for DMF and resulted in good agreement with experiment.[9] Experimental and computational studies demonstrate that FA forms a strongly hydrogen bonded complex with water.[28−30] The microwave spectrum of the 1:1 FA−H_2O complex has been observed and is consistent with a nearly planar structure with two hydrogen bonds, one between the carbonyl oxygen and a water proton and the other between the water oxygen and an amino proton.[28] Recent calculations place the dissociation energy of the complex at 8−9 kcal mol^{-1}.[29,30] No structural studies of FA in water have been reported. However, since the energy required to dissociate the complex is greater than *kT*, it is reasonable to conclude that the 1:1 complex predominates in aqueous solution as well.

Studies of medium effects on conformational processes usually assume statistical kinetics. Our recent study of the internal rotation kinetics of gaseous FA report that the kinetics are pressure dependent at pressures below 3.2 atm.[14] Additional rate constants obtained at pressures between 3 and 23 atm do not show a significant dependence on total system pressure.[31] The reported Arrhenius activation parameters, $E_{act.} = 16.6(0.3)$ kcal mol^{-1} and $A = 1.60(1.02) \times 10^{13}$ s^{-1}, are consistent with Eyring parameters for internal rotation in the high-pressure unimolecular limit of $\Delta G^{\ddagger} = 16.0(0.1)$ kcal mol^{-1}, $\Delta H^{\ddagger} = 15.8(0.6)$ kcal mol^{-1}, and $\Delta S^{\ddagger} = -0.7(0.9)$ cal mol^{-1} K^{-1}, in good agreement with the most recent theoretical calculations. It is not clear at present whether the process is statistical in the gas phase, but the relatively good agreement between the calculated and observed $\Delta S^{\ddagger}$ values indicates that deviations may not be significant. $\Delta S^{\ddagger}$ is negative due to the increase in the NH_2 deformation frequency in TS1. Nonequilibrium behavior in solution can also affect rate constants and kinetic parameters.[32] According to the SCRF model, the effect on the rotational barrier in well-behaved solvents should display a linear dependence with the Onsager dielectric function, $(\epsilon - 1)/(2\epsilon + 1)$, where ϵ is the dielectric constant of the solvent. Deviation may indicate nonequilibrium solvation effects on the rotational barrier.[27] Until more studies are performed and we have a better understanding of nonstatistical effects on low-energy processes, we believe it is prudent to report and interpret results of conformational interconversion studies assuming the kinetics is statistical but to always be aware that this approach may not always be quantitatively correct.

The present study determines experimental internal rotation barriers for FA in three solutions and compares them with model predictions. Experimental NMR measurements were made on samples of the ^{15}N labeled isotopomer to circumvent the broadening of the proton resonances due to interaction with the quadrupole nucleus, ^{14}N. To model the dependence of the rotational barrier of FA on the solute/solvent electrostatic dynamics, we used SCRF theory and polarizable continuum models. The Gaussian 94[33] package includes several methods for SCRF calculations, including the IPCM and SC-IPCM models based on Tomasi's polarizable continuum model. We investigated the energetics of solvated FA using SC-IPCM methods for a range of solvent dielectric constants to test the accuracy of the modeling scheme. To incorporate the specific interactions of FA with a water molecule, computations were performed for an isolated and aqueous solution phase 1:1 FA−H_2O complex.

Experimental Section

Sample Preparation. Solution-phase samples of 1 mol % [^{15}N]FA (Isotec Inc.) were prepared in 5 mm o.d. Wilmad NMR tubes containing either dimethyl sulfoxide-d_6 (DMSO-d_6, Aldrich) or tetrachloroethane-d_2 (TClE-d_2, Aldrich). A 5 mol % sample of [^{15}N]FA was similarly prepared in H_2O. All samples contained a drop of tetramethylsilane (TMS) or dimethyl sulfoxide as a frequency and resolution reference. Solvents and amide were degassed by successive freeze−pump−thaw cycles prior to sample preparation.

Spectroscopic Measurements. Solution-phase ^{1}H NMR spectra were acquired with a wide-bore GE NT-300 spectrometer (proton observation at 300.07 MHz) fitted with a Tecmag acquisition upgrade and equipped with a Bradley 5 mm proton probe. All measurements were made on spinning samples in unlocked mode. Acquisition parameters were as follows: pulse length, 14 μs (90° flip angle); delay time, 5 s; and acquisition time, 3.28 s. Typically 25−50 transients were collected at each temperature and stored in 16 K of memory to achieve a maximum signal-to-noise ratio of 100:1 after multiplication by an exponential line broadening factor of 1 Hz. A sweep width of ±2500 Hz was employed, giving a digital resolution of 0.30 Hz/point. Temperatures were controlled with a 0.1 °C pyrometer and read after each acquisition. Temperature measurements were made using a copper−constantan thermocouple placed within a 5 mm o.d. NMR tube containing TClE-d_2. This closely resembles the experimental setup. All samples were allowed to equilibrate for 30 min prior to acquisition and showed no temperature gradient within the probe's active volume.

Parameter Evaluation. In this and following discussions, the three FA protons will be designated H_A, H_B, and H_C, respectively, where H_A is the amino proton syn to the carbonyl, H_B is the amino proton anti to the carbonyl, and H_C is the formyl proton. Exchange rate constants of [^{15}N]FA, an ABCX spin system, were calculated using the computer program DNMR5[34] which uses an iterative nonlinear least squares regression analysis to obtain the best fit of the experimental ^{1}H NMR spectra. The program was provided with proton chemical shifts at the limit of slow exchange (adjusting for any temperature dependence where applicable), coupling constants, transverse relaxation times, and the digitized NMR spectrum. The effective line width parameter was measured at slow and fast exchange for neat [^{15}N]FA, [^{15}N]FA in TClE-d_2, and [^{15}N]FA in DMSO-d_6 and was estimated in the exchange region by assuming a linear temperature dependence. Fast exchange of [^{15}N]FA in H_2O was beyond the boiling point of the solvent; therefore the effective line width was measured only at a series of slow exchange temperatures. The line width of the reference at each exchange temperature was used to estimate the magnetic field inhomogeneity contribution to the line width. The line width contribution from intermolecular exchange of the amino protons with H_2O for [^{15}N]FA in aqueous solution was estimated by measurement of the line width of the two outermost lines of the formyl proton multiplet.[12] These resonances are unaffected by intramolecular exchange, but they broaden due to intermolecular exchange and their line widths yield the contribution to the total signal broadening due to intermolecular proton exchange. (The frequency difference between the outer lines of the H_C multiplet is the sum of three coupling constants, J_{NC}, J_{AC}, and J_{BC}. Rapid intramolecular exchange makes J_{AC} and J_{BC} equal but does not change their sum and does not change the positions of the outer lines of the multiplet.) Contributions to line widths from field inhomogeniety, the exponential line broadening factor, and intermolecular exchange (for [^{15}N]FA in water) were added to the interpolated (or for [^{15}N]FA in water, extrapolated) effective line width to obtain the total line broadening not due to intramolecular exchange, and thus the effective transverse relaxation time (T_2) for each simulation. Rate constants in the exchange region were obtained by iterating on the rate constant, spectral origin, base-line height, and base-line tilt. All other parameters were held constant.

Computational Methods

Full geometry optimizations of the ground electronic state of the equilibrium structure and the two transition states of isolated FA were performed at the HF/6-311++G** level of theory with zero-point and thermal corrections evaluated using the HF/6-311++G** harmonic frequencies at 298 K and 1 atm. The calculated frequencies were scaled by the conventional factor of 0.893.[35,36] Diffuse functions (+) were included to accurately represent the lone pairs.[37] Computations of the ground state, TS1, and TS2 of the isolated FA−H_2O complex were also performed at this level of theory. MP2/6-31+G* calculations of the ground state and TS1 for the isolated complex were also done. There were no significant differences in the relative energies of the ground state and TS1 for the two methods, we therefore chose to continue our investigation at the HF/6-311++G** level in the interest of computational efficiency.

To obtain the stationary structures of FA in solution, self-consistent reaction field theory calculations using the IPCM and SC-IPCM models were performed. Both methods place the solute in a cavity defined to be an isosurface of the molecule surrounded by a dielectric medium. SC-IPCM differs from IPCM in that it takes into account the coupling between the isosurface and the electron density, allowing for the effects of solvation to be computed directly in the SCF problem. The calculations were done at the HF/6-311++G** level of theory with a 0.001 electron charge/(Bohr radius)^3 (e/B^3) isodensity surface to define the size of the solute cavity and for a series of dielectric constants (5, 10, 20, 30, 40, 78.5, 109). Although studies by Rablen et al. report the model to be relatively insensitive to the isodensity value, they conclude that the most appropriate value of the isodensity contour is 0.001 e/B^3.[27] The two models displayed marked differences in the relative energies calculated. The IPCM model does not allow for complete geometry optimization in the presence of solvent and overestimates the rotational barrier through both TS1 and TS2 with the greatest difference occurring for the rotation occurring via TS2. This is attributed to the greater stabilization of the more polar ground-state and TS2 structures compared to TS1 and is not accurately represented in the IPCM calculations. The SCRF calculations for FA−H_2O were therefore only computed using the SC-IPCM model. These calculations were performed at an isosurface of 0.001 e/B^3, but only for a dielectric constant of 78.5 corresponding to water at 298 K.

All calculations were performed using Gaussian 94.

Results and Discussion

This section is divided into five parts. Parts 1 and 2 describe the NMR data and kinetic parameters for FA in water and in other solvents and as neat solution. These results are summarized in Tables 1−3 and Figures 1 and 2. Parts 3 and 4 describe computational studies which are summarized in Tables 4−6 and Figures 3 and 4. Part 5 compares the experimental results with the calculations. These results are summarized in Figures 5−7.

(1) [^{15}N]FA in H_2O. Since self-aggregation can affect internal rotation rate constants in concentrated solutions,[38] we examined 5 and 1 mol % FA solutions in the current investigation.

TABLE 2: Experimental Limiting Chemical Shifts (ppm) and Spin−Spin Coupling Constants (Hz) for 1 mol % [^{15}N]FA in TClE-d_2 and DMSO-d_6, 5 mol % [^{15}N]FA in Water and as Neat Solution at 298 K[a]

solvent	H_2O	TClE-d_2	DMSO-d_6	neat
δ_A	6.92	6.24	7.16	7.11
δ_B	7.31	5.99	7.43	7.32
δ_C	7.85	8.15	7.99	7.96
J_{AB}	2.14	2.74	2.59	2.20
J_{AC}	13.74	13.71	13.73	13.74
J_{BC}	2.14	1.20	1.83	2.11
J_{AN}	89.12	88.20	86.68	88.35
J_{BN}	91.55	90.00	88.66	90.61
J_{CN}	13.73	16.79	15.30	14.72

[a] A, B, and C refer to amino protons syn to the carbonyl oxygen, anti to the carbonyl oxygen, and the formyl proton. The neat and water solutions are referenced to internal dimethyl sulfoxide ($\delta = 2.5$ ppm), and the TClE-d_2 and DMSO-d_6 solutions, to internal TMS ($\delta = 0.00$ ppm).

Experimental chemical shifts and coupling constants are listed in Table 2. Slow-exchange proton NMR spectra of 5 mol % [^{15}N]FA in H_2O consist of three multiplet resonances downfield from dimethyl sulfoxide ($\delta = 2.5$ ppm) centered at 6.92 and 7.31 ppm corresponding to H_A and H_B ($\delta\nu = 116.27$ Hz) and 7.85 ppm corresponding to the formyl proton, H_C. This is consistent with previous findings of Sunners et al.,[11] Kamei,[12] and Drakenberg and Forsen.[13] Assignment of the resonances is based on the assumption that the trans proton−proton coupling constant, J_{AC}, is greater that the cis coupling constant, J_{BC}. The conclusions of this assignment are independent of these assignments, however. Recent calculations using several first principles quantum mechanical methods predict that the cis coupling is larger than the trans coupling constant.[39] Chemical shifts of FA in water are considerably different from gas-phase values. We previously observed the gas-phase resonances of the amino and formyl protons centered 4.53 and 8.12 ppm downfield from gas-phase TMS.[14] The proton resonances of [^{15}N]FA in H_2O occur at much lower field relative to the dissolved reference, indicating strong intermolecular effects on the nuclear shielding constants. It has been suggested that the degree of planarity and N−H bond lengths can be altered in strongly hydrogen bonded systems, possibly changing the relative screening constants relative to the gaseous state.[40] The spin−spin coupling constants listed in Table 2 agree well with previous measurements[11−13,41] but are also considerably different from gas-phase values. The spin−spin coupling constants for gaseous [^{15}N]FA at fast exchange are $^1J_{NH} = 87.31$ Hz, $^2J_{NH} = 20.14$ Hz, and $^3J_{HH} = 6.71$ Hz. Phase-dependent differences in coupling constants have been attributed to changes in the molecular geometry and molecular charge distributions, but the actual mechanism is not well-understood.[40] The amino ^{1}H chemical shifts of FA in water move upfield as the temperature increases. For H_A and H_B the observed temperature dependences are 0.34(0.02) and 0.37(0.02) ppb K^{-1}. No appreciable temperature dependence is observed for the chemical shift of H_C. J_{AN} and J_{AC} show linear increases with temperature with J_{AN} increasing $7.2(0.8) \times 10^{-3}$ Hz K^{-1} and J_{CN} increasing $9.0(0.5) \times 10^{-3}$ Hz K^{-1}.

Increasing the temperature increases the rate of rotation about the C−N bond, leading to broadening and coalescence of the amino proton resonances. The line shape of the formyl proton resonances changes through the spin−spin interaction with the amino protons. The onset of intermolecular exchange of the amino protons results in further broadening of the proton signals. As was previously mentioned, these two rate processes are separable and accurate determination of the internal rotation rate constants is possible. ^{15}N decoupled spectra[42] were also obtained

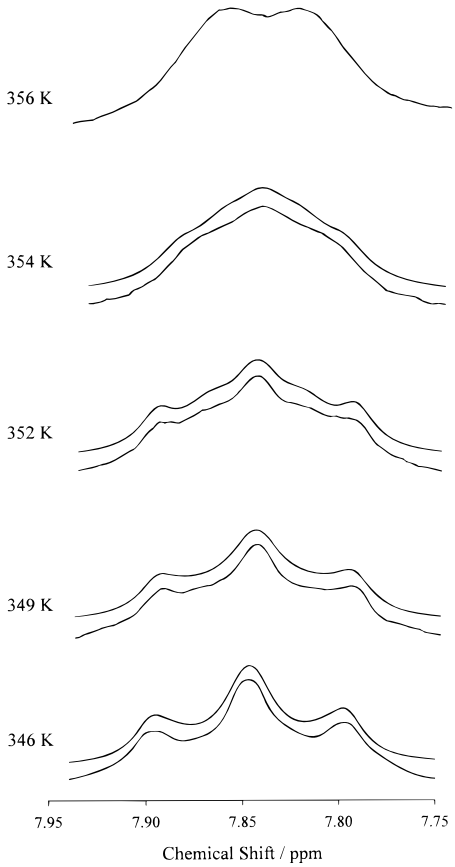

Figure 1. Temperature dependence of the formyl proton resonances of 5 mol % [^{15}N]FA in H_2O at 300 MHz. Top and bottom traces correspond to calculated and experimental spectra. The formyl proton resonance at 356 K shows the intramolecular decoupling of the amino proton resonances.

to simplify the complex spectra and again measure the rotation rate constants. These spectra allowed slightly better measurement of the line width contribution due to intermolecular exchange. The calculated internal rotation rate constants determined from the decoupled spectra at 348.4 and 350.6 K agree very well (within 2%) with the values measured from the coupled spectra.

Exchange broadened spectra of the amino resonances were collected from 355.8 to 366.7 K, and exchange broadened spectra of the formyl proton resonance were collected from 349.1 to 354.1 K. The temperature range where data were collected for the amino proton resonances was limited by overlap with the water proton resonances. Rapid intermolecular exchange of the amino protons with H_2O precluded analysis of the intramolecular rate process from the H_C resonance at temperatures above 354 K due to intramolecular self-decoupling. The intermolecular exchange rate constant at 354 K is estimated at ca. 8 s^{-1} from the experimental J_{AC} and J_{BC} spin−spin coupling constants. Line width measurements of the outermost lines of the H_C resonance from the decoupled spectra in the limit of slow intramolecular exchange yielded intermolecular exchange rate constants of about 3.9 s^{-1} at 340 K and 4.7 s^{-1} at 344 K. These intermolecular exchange rate constants are consistent with an activation energy for FA proton exchange with water of ca. 12.5 kcal mol^{-1}. An earlier study reported an activation energy for proton exchange between FA and water of 14.5(5.5) kcal mol^{-1}.[12] The relatively small line width contribution (<1 Hz) due to intermolecular exchange below 340 K prohibited reliable measurement of the associated rate constant at lower temperatures. Figure 1 shows representative experimental and simulated spectra of H_C. Examination of a 1 mol %

TABLE 3: Experimental Rate Constants (k) to Internal Rotation of 5 mol % [^{15}N]FA in H_2O, 1 mol % [^{15}N]FA in DMSO-d_6 and TClE-d_2, and with Neat Solution as a Function of Temperature

H_2O		DMSO-d_6		TClE-d_2		neat	
T (K)	k (s^{-1})	T (K)	k (s^{-1})	T (K)	k (s^{-1})	T (K)	k (s^{-1})
349.1	35.1(3.0)	348.8	38.2(1.2)	334.6	38.3(0.0)	344.9	28.1(0.4)
352.1	44.9(2.0)	351.8	47.1(1.8)	336.4	44.5(1.2)	247.1	33.0(1.0)
354.1	54.6(5.3)	353.7	53.2(1.3)	337.9	49.0(1.5)	349.4	39.6(0.4)
355.8	60.7(2.1)	354.5	56.7(1.5)	339.7	57.1(0.6)	351.6	46.7(1.0)
358.5	73.6(3.1)	356.0	63.7(1.9)	340.4	59.9(1.7)	353.3	53.4(0.5)
359.4	80.2(2.8)	358.6	75.3(1.7)	341.6	64.5(2.0)	354.0	55.6(0.5)
362.2	96.9(2.3)	360.2	85.1(2.5)	343.9	77.7(1.2)	356.1	65.6(0.6)
364.0	111.8(3.1)					357.7	73.8(0.8)
366.7	140.9(3.2)					359.4	85.4(0.7)

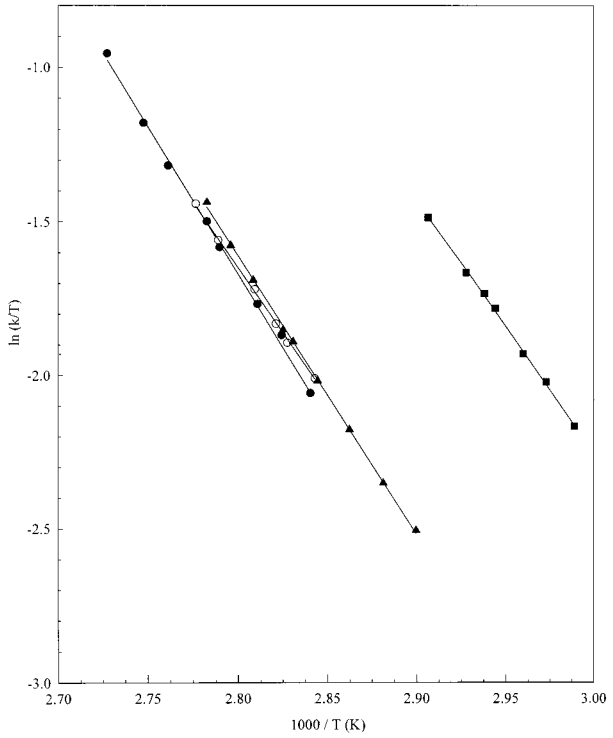

Figure 2. Eyring plots of solvated exchange rate constants of [^{15}N]FA in water (●), DMSO-d_6 (○), and TClE-d_2 (■), and as neat solution (▲).

[^{15}N]FA water solution at 351.1 and 358.3 K showed nearly identical spectra and calculated rate constants indicating complete solvation by H_2O at 5 mol % and no amide aggregation. Temperature-dependent experimental intramolecular rate constants are listed in Table 3 and are shown graphically in Figure 2. Perrin et al. reported the rate constant for internal rotation at 321.1 K (≈3 s^{-1}) for an aqueous solution of [^{15}N]FA, which is in good agreement with rate constants determined in the present study.[43] The Eyring[44] activation parameters determined from the temperature dependence of the internal rotation rate constants are listed in Table 1. The Arrhenius parameters are $E_{act.}$ = 19.7(0.3) kcal mol^{-1} and ln A = 31.8(0.2). $E_{act.}$ is ca. 1.6 kcal mol^{-1} lower than the value reported in 1968 using double resonance experiments $^1H\{^{14}N\}$ of hydrated FA. In that study, spectra were obtained at 40 MHz and spectral analysis accomplished on the basis of an ABC spin system using the method based on bandwidths.[12] This method has been shown to yield rate constants with very large errors.[38] This study was also performed on a 22.8 mol % FA solution in H_2O. It has been suggested that rotational barriers change with high amide concentration (>15 mol %) due to amide aggregation in solution systems; therefore the reported $E_{act.}$ may not accurately represent the H_2O solvated FA system.[45]

TABLE 4: SCF and SC-IPCM Calculated Energies (HF/6-311++G) of Formamide**

molecule	ϵ	ZPE[a] (kcal mol^{-1})	energy[b] (hartrees)	rel energy[c] (hartree)	dipole moment (D)
FA, ground state	1	27.23	−168.892 2962	0	4.218
FA, TS1	1	26.92	−168.869 1516	0.023 14	1.662
FA, TS2	1	26.78	−168.863 6911	0.028 60	4.114
FA, ground state	5	27.41	−168.906 3362	−0.014 04	5.241
FA, TS1	5	26.92	−168.879 2880	0.013 00	2.064
FA, TS2	5	26.83	−168.878 8504	0.013 44	5.092
FA, ground state	10	27.43	−168.908 8433	−0.016 54	5.455
FA, TS1	10	26.92	−168.881 1482	0.010 81	2.142
FA, TS2	10	26.84	−168.881 5332	0.010 76	5.298
FA, ground state	20	27.44	−168.910 1886	−0.017 89	5.566
FA, TS1	20	26.92	−168.882 1325	0.010 16	2.185
FA, TS2	20	26.84	−168.883 0146	0.009 28	5.416
FA, ground state	30	27.44	−168.910 6518	−0.183 56	5.611
FA, TS1	30	26.92	−168.882 4717	0.009 82	2.199
FA, TS2	30	26.84	−168.883 5343	0.008 79	5.456
FA, ground state	40	27.45	−168.910 8862	−0.185 90	5.631
FA, TS1	40	26.91	−168.882 6441	0.009 65	2.207
FA, TS2	40	26.94	−168.883 7995	0.008 49	5.477
FA, ground state	50	27.45	−168.911 0278	−0.018 73	5.644
FA, TS1	50	26.92	−168.882 7477	0.009 54	2.209
FA, TS2	50	26.84	−168.883 9601	0.008 33	5.490
FA, ground state	78.5	27.45	−168.911 2346	−0.018 93	5.659
FA, TS1	78.5	26.92	−168.882 8951	0.009 40	2.216
FA, TS2	78.5	26.84	−168.884 1912	0.008 10	5.509
FA, ground state	109	27.45	−168.911 3367	−0.190 40	5.668
FA, TS1	109	26.92	−168.882 9689	0.009 32	2.219
FA, TS2	109	26.84	−168.884 3061	0.007 99	5.518

[a] ZPE corrections used vibrational frequencies scaled by 0.893. [b] Total energy including thermal and ZPE corrections at 298.15 K. [c] Energies relative to gas-phase ground state.

(2) [^{15}N]FA in DMSO-d_6, TClE-d_2, and Neat FA. Experimental NMR parameters of [^{15}N]FA in DMSO-d_6, TClE-d_2, and neat FA are summarized in Table 2. Again assignment of the proton resonances is based upon the magnitude of the cis and trans proton−proton coupling constants. Amino proton chemical shifts of all three samples display a linear temperature dependence to higher field. The amino proton chemical shifts in DMSO-d_6 show a temperature dependence of 0.41(0.06) ppb K^{-1} for H_B and 0.36(0.08) ppb K^{-1} for H_A. The amino proton chemical shifts in TClE-d_2 showed a temperature dependence of 0.35(0.05) ppb K^{-1} for both the high- and low-field resonances. For the neat solution, the temperature dependence of the chemical shifts was 0.30(0.05) ppb K^{-1} and for both the high-field and low-field amino resonances. No temperature dependence of the H_C resonance was observed in these solutions. Measurable broadening of the H_C resonance due to intermolecular exchange was not observed for neat FA below 384 K. Since this temperature is in the fast exchange limit, determining rate constants for the internal rotation process was not complicated by the intermolecular exchange process. Complete intramolecular decoupling of the amino resonances of neat FA was observed at 398.2 K, consistent with an intermolecular exchange rate constant of 8 s^{-1}. Similar decoupling was observed at 354 K for FA in water, indicating that hydrogen exchange between water and FA is more facile than between FA molecules. No intermolecular exchange broadening was observed for the DMSO-d_6 and TClE-d_2 solutions.

Exchange broadened spectra of the H_C resonance of these [^{15}N]FA systems were collected from 348.8 to 360.2 K (DMSO-d_6), from 334.6 to 344.0 K (TClE-d_2), and from 344.9 to 358.5 K (neat solution). Examination of 0.1 mol % FA solutions at

TABLE 5: SCF and SC-IPCM Calculated Eyring Parameters for C−N Internal Rotation of FA and FA−H_2O at 298.15 K ($\Delta H^{\ddagger}$ and $\Delta G^{\ddagger}$ in kilocalories per mole and $\Delta S^{\ddagger}$ in calories per mole per kelvin)

	$\epsilon = 1.0$				$\epsilon = 78.5$			
molecule	$\Delta G^{\ddagger}$	$\Delta H^{\ddagger}$	$\Delta S^{\ddagger}$	$\Delta G^{\ddagger}$(combined)	$\Delta G^{\ddagger}$	$\Delta H^{\ddagger}$	$\Delta S^{\ddagger}$	$\Delta G^{\ddagger}$(combined)
FA(TS1)	15.26	14.52	−2.48	15.25	18.17	17.78	−1.28	17.24
(TS2)	18.70	17.95	−2.55		17.38	16.97	−1.38	
FA−H_2O (TS1)	16.77	15.30	−4.93	16.74	18.56	17.63	−3.11	17.57
(TS2)	18.62	17.71	−3.05		17.70	16.87	−2.83	

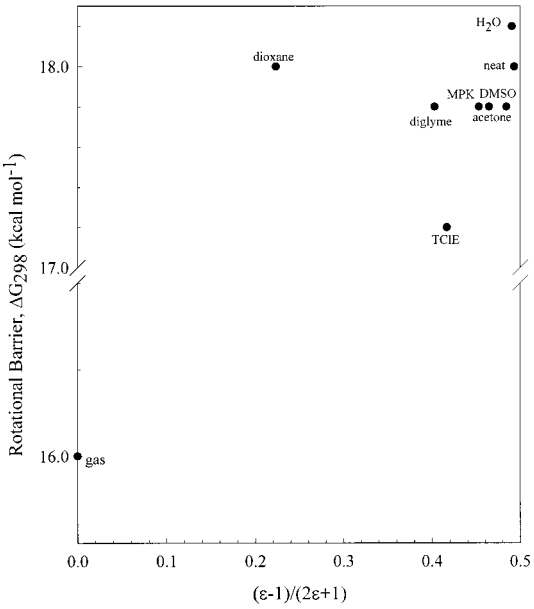

Figure 3. Onsager plots of the calculated rotational barriers, $\Delta G^{\ddagger}_{298}$, via the SC-IPCM (HF/6-311++G**) method.

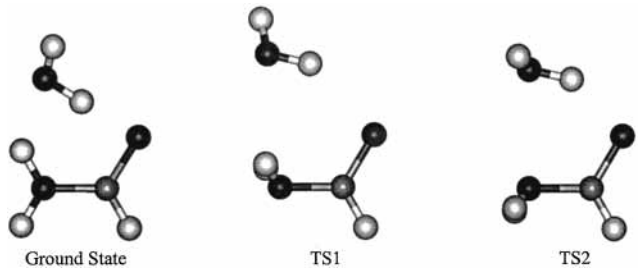

Figure 4. FA−H_2O complex configuration of the ground state, TS1, and TS2 from the Gaussian SC-IPCM (HF/6-311++G**) optimized geometries.

337.9 and 340.4 K for the TClE-d_2 system and 353.7 and 356.0 K for the DMSO-d_6 system yielded similar rate constants compared to the 1 mol % solutions, indicating complete solvation and no amide aggregation. Exchange rate constants were also calculated using the amino proton resonances for these systems at various temperatures. These values were in excellent agreement with the values obtained from the formyl data. Temperature-dependent internal rotation rate constants are listed in Table 3 and shown graphically in Figure 2. The Eyring activation parameters are listed in Table 1. For the samples studied, the FA internal rotation barrier increases with increasing solvent polarity and hydrogen bonding capability.

(3) SC-IPCM Calculations of FA. The results of a series of calculations using SC-IPCM are presented in Table 4. The energies of the ground state, TS1, and TS2 decrease with increasing solvent polarity. This effect is greatest for the ground state and for TS2, which are both significantly more polar than TS1. Increasing the solvent polarity reduces the barrier to rotation proceeding via TS2 and increases the barrier to rotation proceeding via TS1. The calculated Eyring parameters for internal rotation are listed in Table 5. The calculated $\Delta G^{\ddagger}_{298}$ values for the TS1 reaction pathway increase (slope = 5.92) linearly with the Onsager dielectric function $(\epsilon - 1)/(2\epsilon + 1)$ while the $\Delta G^{\ddagger}_{298}$ values for the TS2 path decrease (slope = −2.68) as shown in Figure 3.

Figure 3 also demonstrates a reversal of the predicted lowest energy reaction pathway in polar solvents. In the absence of solvent the reaction proceeds almost exclusively via TS1; however, introduction of solvent leads to a 50:50 reaction pathway via TS1 and TS2 at $\epsilon = 7.08$. Further increase in solvent polarity leads to an increase in the contribution of TS2 to the total rate process and a decrease in TS1. The calculations predict TS2 to be the primary reaction channel for aqueous FA, consistent with previous findings by Craw et al.[5] Studies reported by Wiberg et al. report similar but less dramatic results for IPCM calculations of DMA.[9] These studies show TS1 to be the favored reaction path for gaseous DMA with increasing contribution from TS2 with increasing solvent polarity. The total rate process appears to have significant mixing of the two reaction channels; however, no reversal is reported. The similarity between FA and DMA arises from the preferred TS1 path in the gas phase, and because TS1 has a smaller dipole moment than TS2, polar solvents increase the TS2 preference. The pronounced preference of TS2 for FA in polar solvents compared to DMA is due to the increased dipole moment difference of the ground-state and TS1 conformers. The calculated dipole moments for isolated DMA are 3.93, 2.12, and 3.75 D for the ground state, TS1, and TS2, respectively. Wiberg et al. also reported IPCM predictions for DMF. In this case the more polar transition-state path, TS2, is always the operative one.

(4) FA−H_2O Complex Calculations. Full geometry optimizations for the isolated complex and for the complex in a medium with a dielectric constant of 78.5, corresponding to water at 298 K, were performed at the HF/6-311++G** level of theory. The calculations predict a cyclic minimum energy complex structure, shown in Figure 4, with simultaneous hydrogen bonds with the water molecule at the carbonyl oxygen and at the cis amino hydrogen, consistent with previous computational and experimental investigations.[46−50] The experimentally derived geometry of the ground-state FA−H_2O complex reported by Lovas et al.[28] shows that the intermolecular hydrogen bond lengths for the amide hydrogen bond to the hydroxyl oxygen and the carbonyl interaction are nearly identical, indicating a doubly hydrogen bonded complex. Their studies also report a negative calculated inertial defect indicative of a slightly nonplanar complex. They conclude that the nonbonded hydrogen of the water molecule is tilted approximately 17° out of the plane of the heavy atoms. No appreciable change in the experimental and calculated monomer geometries were observed with the addition of the water molecule for the isolated complex. There are, however, small changes in the SC-IPCM optimized geometries. Both the isolated and SC-IPCM complexes show small changes in the orientation of the water molecule with rotation, as is illustrated in Figure

4. The calculated binding energies are −8.31 kcal mol^{-1} for the ground state, −7.91 kcal mol^{-1} for TS1, and −8.05 kcal mol^{-1} for TS2. The increased binding energy for the equilibrium structure and TS2 indicates stronger hydrogen bonding compared to TS1. Previous reports of the binding energy for the ground-state complex range from −4.6 to −11.4 kcal mol^{-1}.[46−50] No previous estimations of the complex binding energies for the transition states have been reported in the literature.

The predicted thermal and zero-point energy (ZPE) corrected Eyring parameters listed in Table 5 show that $\Delta G^{\ddagger}_{298}$ for internal rotation of the gas-phase 1:1 FA−H_2O complex proceeding via TS1 is ca. 1.5 kcal mol^{-1} higher than that for gas-phase uncomplexed FA, while $\Delta G^{\ddagger}_{298}$ for internal rotation via TS2 is essentially independent of complexation. The increase in $\Delta G^{\ddagger}_{298}$ for internal rotation via TS1 is due to increased stabilization of the ground state relative to TS1 and the unchanged $\Delta G^{\ddagger}_{298}$ for internal rotation via TS2 indicates the same degree of stabilization occurs for the ground state and TS2. Previous calculations performed by Wang et al.[49] and Chen and Gordon[7] report a 2−3 kcal mol^{-1} increase above the monomer barriers (TS1), consistent with our current findings. To our knowledge, no computational investigation of the barrier for the 1:1 FA−H_2O complex via the TS2 reaction pathway has been reported.

Direct inclusion of hydrogen bonding in the SC-IPCM calculation was done by placing the FA−H_2O complex in the dielectric cavity ($\epsilon = 78.5$). This method has been previously applied to hydrated DMF, yielding a predicted barrier closer to the experimental value.[9] The SC-IPCM computed thermodynamic values for the complex in water show a 0.3 kcal mol^{-1} increase in barrier height above the hydrated monomer for the reaction proceeding via the favored TS2 reaction pathway. To compare the theoretical and experimental rotational barriers of solvated FA, it is first necessary to determine a net $\Delta G^{\ddagger}_{298}$ (combined) that takes into account the combined effects on the rotation rate constant from both reaction pathways. The net $\Delta G^{\ddagger}_{298}$ (combined) value for the hydrated complex is ca. 2.3 kcal mol^{-1} higher than the predicted gas-phase value, in excellent agreement with the experimental difference of 2.2 kcal mol^{-1}.

(5) Experimental Correlation. The SC-IPCM $\Delta G^{\ddagger}_{298}$ (combined) values shown in Table 1 increase from the gas-phase prediction with increasing dielectric constant and reach a maximum rotational barrier at ca. $\epsilon = 16.0$. Further increase in dielectric constant leads to a greater contribution from TS2 to the overall rate process, resulting in a decrease in rotational barrier. The $\Delta G^{\ddagger}_{298}$(combined) values predicted are consistently lower than the experimental values with the greatest underestimation of the solvated barrier for the neat solution and FA in dioxane and water. IPCM calculations of DMA and DMF also underestimate the barrier (≈10%). The underestimation of the barriers for the H_2O and neat solutions is not surprising considering the strong hydrogen bonding in these systems which is not explicitly included in the SC-IPCM calculations. The large underestimation of the predicted barrier in dioxane is probably the result of high amide concentration (24.6 mol % FA). The observed rotational barrier may be complicated by amide self-association. The net $\Delta G^{\ddagger}_{298}$(combined) for hydrated FA is 1.99 kcal mol^{-1} higher than the predicted gas-phase value. Craw et al. predict a 1.34 kcal mol^{-1} increase above the isolated value, possibly indicating basis set dependence on the calculated energies. To further explore this, we computed the aqueous barrier using SC-IPCM (HF/6-31+G*), which yielded a barrier (17.859 kcal mol^{-1}) 1.87 kcal mol^{-1} higher than the gas-phase prediction at the same level (15.988 kcal mol^{-1}). Because the internal rotational process is driven by the interaction of the electron deficient carbon and the nitrogen lone pair, we conclude that the calculations which include diffuse function (+) better represent the energetics of the process.

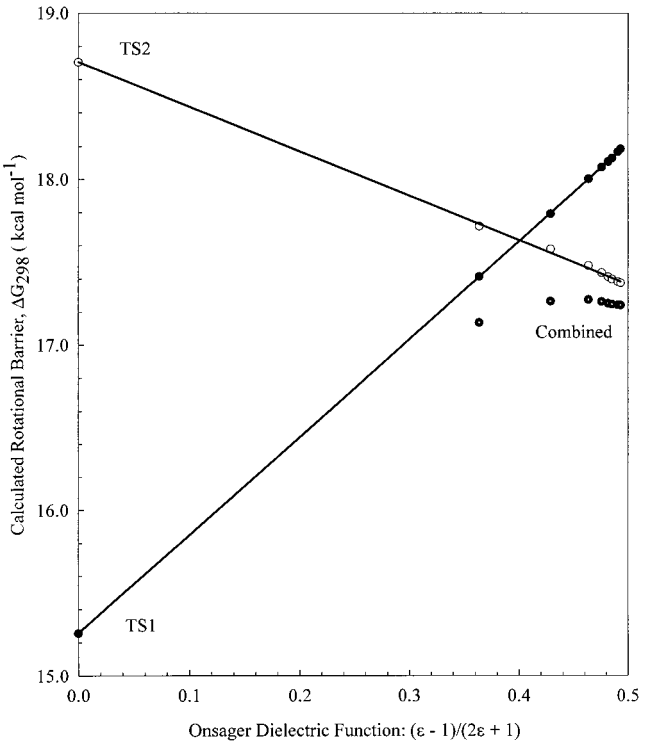

Figure 5. Correlation of the experimental rotational barriers, $\Delta G^{\ddagger}_{298}$, of FA with the Onsager dielectric function.

It has been previously shown that the rotational barriers in DMA and DMF yield essentially linear relationships with the Onsager dielectric function for solvents that do not strongly hydrogen bond, are not aromatic, and are not halogenated.[27] The correlation of the experimental $\Delta G^{\ddagger}_{298}$ values for FA with the Onsager dielectric function is shown graphically in Figure 5. Experimentally determined barriers for FA in dioxane, diglyme, TClE-d_2, methyl propyl ketone (MPK), acetone, DMSO-d_6, and H_2O, as neat solution, and in the gas-phase are shown. The close correlation in MPK, diglyme, acetone, and DMSO-d_6 indicates a bulk dielectric effect on the rotational barrier for FA consistent with statistical kinetics. The remarkable different dioxane and TClE-d_2 barriers are attributed to high amide concentration (dioxane) and stronger than expected interactions for the halogenated solvent (TClE-d_2). Halogenated solvents, such as TClE, may have stronger than expected short-range interactions because of the greater electron polarizability of the chlorine atoms yielding large, unexpected effects on the rotational barrier.[9,26−27] This is observed in the present study. The same observation has been made in the Onsager treatments of the DMA and DMF in carbon tetrachloride. The neat and H_2O solutions show barriers much higher than the well-correlated values due to strong intermolecular hydrogen bonding effects.

The effects of solvent polarity were also investigated through analysis of the correlation of the experimental rotational barriers with empirical solvent polarity scales. Wiberg's study of DMF reports excellent correlation of the solvated internal rotation barriers with E_t, a spectroscopic solvent polarity parameter developed by Dimroth and co-workers (Figure 6).[3] Our analysis of the reported DMA data also shows excellent correlation with E_t. Figure 6 illustrates the same correlation of the experimental

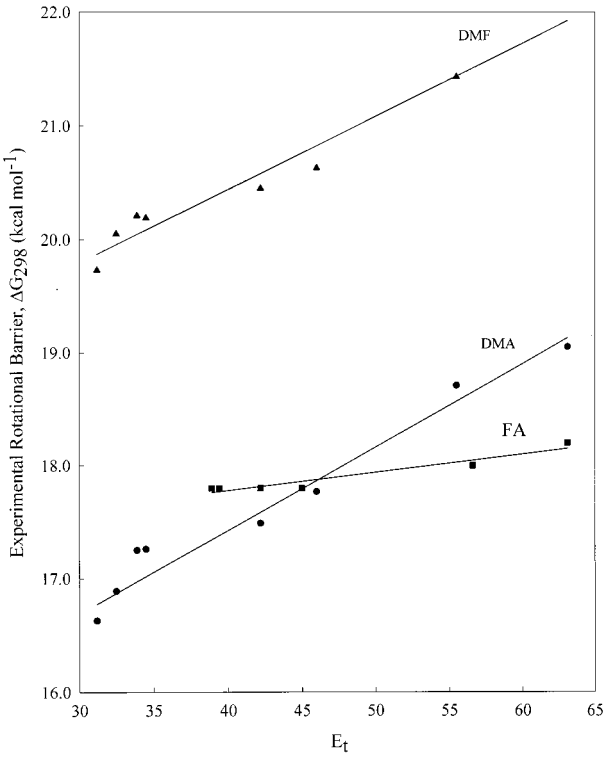

Figure 6. Correlation of the experimental rotational barriers, $\Delta G^{\ddagger}_{298}$, with empirical solvent polarity parameter, E_t. The equations of the best fit lines for the three solvated systems are as follows: DMF, $\Delta G^{\ddagger}_{298}$ (kcal mol^{-1}) = 4.02(0.31)E_t + 21.18(0.08); DMA, $\Delta G^{\ddagger}_{298}$ (kcal mol^{-1}) = 5.44(0.25)E_t + 18.34(0.07); FA, $\Delta G^{\ddagger}_{298}$ (kcal mol^{-1}) = 3.23(0.31)E_t + 17.74(0.73).

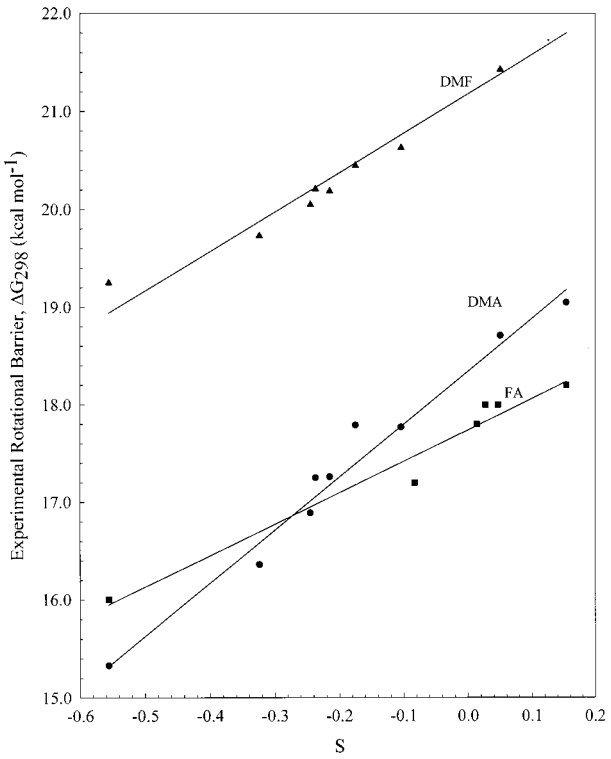

Figure 7. Correlation of the experimental rotational barriers, $\Delta G^{\ddagger}_{298}$, with empirical solvent polarity parameter, S. The equations of the best fit lines for the three solvated systems are as follows: DMF, $\Delta G^{\ddagger}_{298}$ (kcal mol^{-1}) = 0.64(0.04)S + 17.86(0.21); DMA, $\Delta G^{\ddagger}_{298}$ (kcal mol^{-1}) = 0.07(0.01)S + 14.47(0.34); FA, $\Delta G^{\ddagger}_{298}$ (kcal mol^{-1}) = 0.02(0.01)S + 17.14(0.11).

solvated FA rotational barriers with E_t. The data for DMF, DMA, and FA show similar correlation with Brownstein's solvent parameter, S, which represents a statistical average of several spectroscopic solvent polarity parameters (Figure 7).[51] Both treatments suggest that the absorption of light by a solvated dye is governed by the same properties affecting amides during bond rotation. The electronic excitation of the dye chromophore and the C−N bond rotation are both largely dependent on the relative polarity and intermolecular interactions, such as hydrogen bonding, of the ground and excited states.

It has also been suggested that such close correlation exists because the electronic excited state of the dye and the transition state to bond rotation are both characterized by nonequilibrated solvation configurations.[27] Solute structure changes very fast during electronic excitation, resulting in an initial nonequilibrated solvation condition of the excited state. Although the C−N bond rotation is a relatively "slow" process, actual molecular motions required for the internal rotation process are on the vibrational time scale. Because the time required for solvent reorganization is on the translational/rotational time scale, solvation of the transition state may not be completely equilibrated. It is therefore probable that the solvent molecules retain the relatively same arrangement throughout the C−N bond rotation process. Dielectric friction is the dynamic effect responsible for the slowness of solvent molecule reorientation.[52] SC-IPCM computation will therefore lead to a solvation energy too favorable due to the equilibrium treatment of the transition state. Equilibration is implied by use of a static dielectric constant. This is consistent with the constant underestimation of the SC-IPCM calculated rotational barriers because the computational method assumes an equilibrium minimum energy solvation state for all structures along the reaction path.

The effects of nonequilibrium solvation (dielectric friction) will be the greatest for solutes with substantially different ground- and transition-state structures. In a previous study, Rablen[27] and co-workers concluded that DMAAN experiences greater nonequilibrium effects compared to DMA due to the increased differences in dipole moment magnitude and orientation upon rotation of DMAAN via the more favorable TS2 reaction pathway. The calculated dipole moments of isolated DMAAN are 6.655 D (ground state), 4.223 D (TS1), and 4.480 D (TS2). Rablen et al. reported changes in dipole moment magnitude of 3.312 and 2.168 D for DMAAN (TS2) and DMA (TS1), respectively. The calculated change in dipole moment magnitude for FA is 2.632 D (TS1). Nonequilibrium effects in FA should be intermediate between DMAAN and DMA. The DMAAN and DMA calculations underestimate the barrier in water by ca. 30 and 10%, respectively. The present study reports a ca. 6% underestimate of the rotational barrier for hydrated FA. Assuming the solvent molecules remain in relatively the same arrangement upon rotation, the greater agreement between the calculated and experimental FA barriers compared to DMA suggests the latter actually experiences greater destabilization due to nonequilibrium effects of the solvent molecules at the transition state. QM-MM calculations for DMA−H_2O complexes predict a ground-state structure with a water molecule hydrogen bonded to the carbonyl oxygen.[53] However, upon rotation, the steric interference between the *N*-methyl groups and the water molecule inhibits hydrogen bond donation at the carbonyl oxygen and the lowest energy DMA−H_2O complex in water has the water molecule hydrogen bonded at the nitrogen. QM-MM calculations predict TS2 to be competitive in water. Our FA−H_2O complex calculations show that hydrogen bonding at the carbonyl oxygen is always favored. This would result in less solvent reorganization upon rotation

in comparison to DMA. It is also possible that the better agreement of the FA calculated and experimental barriers is the result of the SCRF model used (SC-IPCM for FA and IPCM for DMA). This study reports considerable differences in the FA calculated barriers computed using these two models.

Summary

Kinetic parameters determined from dynamic ^{1}H NMR studies of neat liquid [^{15}N]FA and [^{15}N]FA in H_2O, DMSO-d_6, and TClE-d_2 combined with previously reported gas-phase and solution results have allowed the effects of solvent polarity and hydrogen bonding capability on the rotational barrier to be determined.

SC-IPCM calculations performed to estimate the electrostatic effects of solvation on the rotational barrier predict a reversal of the lowest energy pathway from TS1 at low-ϵ values to TS2 at higher ϵ values. Calculated $\Delta G^{\ddagger}_{298}$(combined for both reaction paths) values are consistently lower than the experimental values. Experimental barriers for FA in methyl propyl ketone, diglyme, acetone, and DMSO-d_6 correlate well with the Onsager dielectric function. All available experimental values correlate well with empirical spectroscopic solvent polarity scales.

Explicit incorporation of the water molecule in the SCRF calculation yields a good model of the rotation energetics of hydrated FA. SC-IPCM calculations for a 1:1 FA$-H_2O$ complex yielded barriers of 18.56 and 17.70 kcal mol^{-1} for FA internal rotation via TS1 and TS2, respectively. The net $\Delta G^{\ddagger}_{298}$(combined) is ca. 2.3 kcal mol^{-1} higher than the predicted gas-phase value, in excellent agreement with the experimental difference of 2.2 kcal mol^{-1}.

Acknowledgment. The authors are pleased to acknowledge support from the National Science Foundation (Grant CHE 93-21079) for support of this research.

References and Notes

(1) Kyte, J. *Mechanism in Protein Chemistry*; Garland: New York, 1995.
(2) Lehninger, A. L.; Nelson, D. L.; Cox, M. M. *Principles of Biochemistry*; Worth: New York, 1993.
(3) Reichardt, C. *Solvent Effects in Organic Chemistry*; Verlag Chemie: Weinhein, Germany, 1979.
(4) Oie, T.; Topol, I. A.; Burt, S. K. *J. Phys. Chem.* **1995**, *99*, 905.
(5) Craw, J. S.; Guest, J. M.; Cooper, M. D.; Burton, N. A.; Hillier, I. A. *J. Phys. Chem.* **1996**, *100*, 6304.
(6) Burton, N. A.; Chiu, S. S.-L.; Davidson, M. M.; Green, D. V. S.; Hillier, I. H.; McDouall, J. J. W.; Vincent, M. A. *J. Chem. Soc., Faraday Trans.* **1993**, *89*, 2631.
(7) Chen, W.; Gordon, M. S. *J. Chem. Phys.* **1996**, *105*, 11081
(8) Wang, X.-C.; Facelli, J. C.; Simons, J. *Int. J. Quantum Chem.* **1993**, *45*, 123.
(9) Wiberg, K. B.; Rablen, P. R.; Rush, D. J.; Keith, T. A. *J. Am. Chem. Soc.* **1995**, *117*, 4261.
(10) Colominas, C.; Luque, F. J.; Orozco, M. *J. Phys. Chem. A* **1999**, *103*, 6200.
(11) Sunners, B.; Piette, L. H.; Schneider, W. G. *Can. J. Chem.* **1960**, *38*, 681.
(12) Kamei, H. *Bull. Chem. Soc. Jpn.* **1968**, *41*, 2269.
(13) Drakenberg, T.; Forsen, S. *J. Phys. Chem.* **1970**, *74*, 1−7.
(14) Taha, A. N.; Neugebauer Crawford, S. M.; True, N. S. *J. Am. Chem. Soc.* **1998**, *120*, 1934.
(15) Kurland, R. J.; Wilson, E. B. *J. Chem. Phys.* **1957**, *27*, 585.
(16) Staley, R. H.; Harling, L. B.; Goddard, W. A.; Beauchamp, J. L. *Chem. Phys. Lett.* **1975**, *36*, 589.
(17) This work.
(18) Forgasi, G.; Szalay, P. G. *J. Phys. Chem. A* **1997**, *101*, 1400.
(19) Basch, H.; Shmaryahu, H. *Chem. Phys. Lett.* **1998**, *294*, 117.
(20) Keininger, M.; Suhai, S. *J. Mol. Struct.* **1996**, *375*, 181.
(21) Ou, M.-C.; Chu, S.-Y. *J. Phys. Chem.* **1995**, *99*, 556.
(22) Olsen, L. F.; Li, Y.; Houk, K. N.; Kresge, A. J. *J. Am. Chem. Soc.* **1995**, *117*, 2992.
(23) Laidig, K. E.; Cameron, L. M. *Can. J. Chem.* **1993**, *71*, 872.
(24) Wiberg, K. B.; Breneman, C. M. *J. Am. Chem. Soc.* **1992**, *114*, 831.
(25) Tsuzuki, S.; Tanabe, K. *J. Chem. Soc., Perkin Trans. 2* **1991**, 1255.
(26) Rablen, P. R.; Miller, P. A.; Bullock, V. R.; Hutchison, P. H.; Gorman, J. A. *J. Am. Chem. Soc.* **1999**, *121*, 218.
(27) Rablen, P. R.; Pearlman, S. A.; Miller, D. A. *J. Am. Chem. Soc.* **1999**, *121*, 227.
(28) Lovas, F. J.; Suenram, R. D.; Fraser, G. T.; Gillies, C. W.; Zozom, J. *J. Chem. Phys.* **1988**, *88*, 722.
(29) Contador, J. C.; Sanchez, M. L.; Aguilar, M. A.; Olivares del Valle, F. J. *J. Chem. Phys.* **1996**, *104*, 5539.
(30) Engdahl, A.; Nelander, B. *J. Chem. Phys.* **1993**, *99*, 4894.
(31) Taha, A. N.; True, N. S. Manuscript in preparation.
(32) Hynes, J. T. *Annu. Rev. Phys. Chem.* **1985**, *36*, 573.
(33) Frisch, M. J.; Trucks, G. W.; Schlegel, H. B.; Gill, P. M.; Johnson, B. G.; Robb, M. A.; Cheeseman, J. R.; Keith, T.; Peterson, G. A.; Montgomery, J. A.; Raghavachari, K.; Al-Laham, M. A.; Zakrzewski, V. G.; Ortiz, J. V.; Foresman, J. B.; Cioslowski, J.; Stefanov, B. B.; Nanayakkara, A.; Challacombe, M.; Peng, C. Y.; Ayala, P. Y.; Chen, W.; Wong, M. W.; Andres, J. L.; Repogle, E. S.; Gomperts, R.; Gonzalez, C.; Martin, R. L.; Fox, D. J.; Binkley, J. S.; Defrees, D. J.; Baker, J.; Stewart, J. P.; Head-Gordon, M.; Pople, J. A. *Gaussian 94* (Revision B.2); Gaussian Inc.: Pittsburgh, PA, 1995.
(34) (a) Stephensen, D. S.; Binsch, G. Program No. 365. (b) LeMaster, C. B.; LeMaster, C. L.; True, N. S. Programs Nos. 569 and QCMP059; *Quantum Chemistry Program Exchange*; Indiana University: Bloomington, IN 47405.
(35) Curtiss, L. A.; Raghavachari, K.; Trucks, G. W.; Pople, J. A. *J. Chem. Phys.* **1991**, *94*, 7221.
(36) Curtiss, L. A.; Carpenter, J. E.; Ragavachari, K; Pople, J. A. *J. Chem. Phys.* **1992**, *96*, 9030.
(37) Clark, T.; Chandrasekhar, J.; Spitznagel, G. W.; Schleyer, P. v. R. *J. Comput. Chem.* **1983**, *4*, 249.
(38) Sandstron, J. *Dynamic NMR Spectrsocopy*; Academic Press: New York, 1982.
(39) Varra, J.; Kaski, J.; Jokisaari, J.; Diehl, P. *J. Phys. Chem.* **1997**, *101*, 5069.
(40) Buckingham, A. D. *Can. J. Chem.* **1960**, *38*, 300.
(41) Chuck, R. J.; Gilles, D. G.; Randall, E. W. *Mol. Phys.* **1969**, *16*, 121.
(42) The 7 W output from a Wavetek frequency synthesizer was applied to the probe through the lock coil.
(43) Perrin, C. L.; Thoburn, J. D.; Kresge, A. J. *J. Am. Chem. Soc.* **1992**, *114*, 8800.
(44) A transmission coefficient of unity was used in the Eyring analysis.
(45) Duffy, E. M.; Severence, D. L.; Jorgensen, W. L. *J. Am. Chem. Soc.* **1987**, *109*, 3526.
(46) Engdahl, A.; Nelander, B. *J. Chem. Phys.* **1993**, *99*, 4894.
(47) Jasien, P. G.; Stevens, W. J. *J. Chem. Phys.* **1986**, *84*, 3271.
(48) Jorgensen, W. L.; Swenson, C. J. *J. Am. Chem. Soc.* **1985**, *107*, 1489.
(49) Wang, X.-C.; Nichols, J.; Feyereisen, M.; Gutowski, M.; Boatz, J.; Haynet, A. D. J.; Simons, J. *J. Phys. Chem.* **1991**, *95*, 10419.
(50) Rablen, P. R.; Lockman, J. W.; Jorgensen, W. L. *J. Phys. Chem.* **1998**, *102*, 3782.
(51) Brownstein, S. *Can. J. Chem.* **1960**, *38*, 1590.
(52) Waldeck, D. H. *Chem. Rev.* **1991**, *91*, 415.
(53) Duffy, E. M.; Severence, D. L.; Jorgensen, W. L. *J. Am. Chem. Soc.* **1992**, *114*, 7535.